Design and Construction of a Multi-Port Permanent Magnet Synchronous Generator Prototype for an Integrated Generator-Rectifier System

Anjana J. Samarakoon[1], Samith Sirimanna[2], Anubhav Bose[1], Debranjan Mukherjee[3],
Luigi Passerotti[1], Arijit Banerjee[1], Kiruba Haran[1]
[1]Department of Electrical and Computer Engineering, University of Illinois Urbana Champaign, Urbana, IL, USA
Email: {spa5, bose15, luigis2, arijit, kharan}@illinois.edu
[2]Hinetics LLC, Champaign, IL, USA
Email: samith@hinetics.com
[3]Department of Electrical Engineering, Indian Institute of Technology Kharagpur, India
Email: debranjan@ee.iitkgp.ac.in

***Abstract*—Integrated generator–rectifier systems are becoming increasingly popular in applications such as wind energy, where efficiency and low drivetrain size are critical features. Recent studies have demonstrated that tightly integrating the generator with a passive rectification stage can significantly reduce overall system weight while simultaneously improving efficiency. By minimizing the number of active switching devices in the rectification stage, this architecture improves reliability, torque density, and Levelized Cost of Energy over prior state of the art systems. Building on this concept, a multi-megawatt-scale integrated generator–rectifier topology has been proposed and optimized for large wind turbines. To experimentally validate the feasibility of this architecture, a 200 kW laboratory-scale prototype permanent magnet synchronous generator (PMSG) was designed and constructed. This paper presents the design methodology, construction process, and experimental evaluation of this laboratory-scale prototype. Key design choices made to address manufacturability challenges in the PMSG are presented to provide insight for generator designers.**

***Index Terms*—integrated generator-rectifier, slotless generator, torque density.**

I. Introduction

Permanent magnet synchronous generators (PMSG) are becoming an increasingly attractive choice for multi-megawatt class wind turbines [1]. To improve the reliability and efficiency of these wind turbine drivetrains, an integrated generator-rectifier system is proposed in [2], which reduces the rectifier weight, increases the efficiency, and the reliability of the drive by reducing the requirement of active switches, as shown in the Fig. 1. Full power flow control is achievable to extract maximum power [3], [4] even with the majority use of passive switching devices. The architecture comprises of a multi-port generator with specific phase shifts among different ports and low per-unit reactance. A coupled optimization scheme was used to determine the optimum combination of passive and active ports to achieve the highest efficiency at the lowest weight at 10 MW [5]. The final architecture divides the generator AC connections into three 3-phase passive ports and one 3-phase active port. The optimized PMSG design has 240 poles with an estimated torque density of 157 Nm/kg and 97.2% efficiency. These efficiency and torque density numbers are higher than currently available wind turbine generators [6].

To validate this 10 MW concept design at the laboratory scale, a scaled-down prototype is proposed. The prototype generator was designed for 200 kW to match the rating of the University of Illinois high-power motor-drive test bed. This paper focuses on the design, construction, and testing of 200 kW prototype PMSG. In this prototype, the key characteristics of the 10 MW system are scaled appropriately to the 200 kW level. Design characteristics of this scaled prototype are presented in this paper. Specific manufacturability considerations and the associated design directions to maintain the key performance metrics are discussed. Experimental results from the tests of the prototype are presented towards the goal of validating overall system operation.

II. Design of 200 kW PMSG

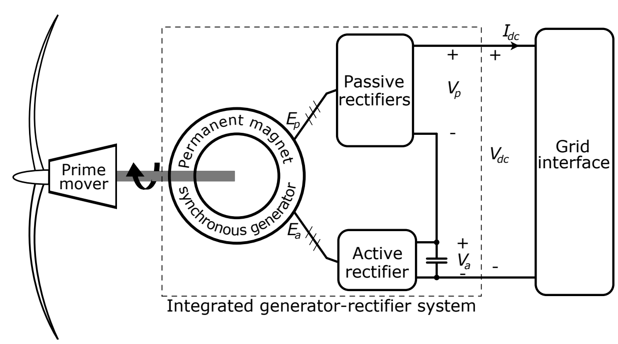

Fig. 1: Integrated multi-port generator-rectifier architecture

The primary objective of this prototype is to validate the 10 MW system architecture at 200 kW scale, with generator performance consistent with scaled expectations from prior 10 MW design studies. The rotational speed, permanent magnet

979-8-3315-8138-1

(PM) volume, and electrical loading were scaled down from the prior 10 MW design to maintain overall MW-level performance metrics and to address manufacturability concerns.

A coupled genetic algorithm and electromagnetic finite-element-based solver was developed based on the optimization procedure described in [5], [6] to find the optimal generator design for a 200 kW prototype. Figure 2 shows the 4-pole-pair cross-section with the rotor shaft, Halback array magnets, air gap, copper winding, and the stator yoke appropriately labeled. Figure 3 shows the PMSG construction. A finite element model (FEA) was used to calculate the induced emf, torque, and flux density inside the stator yoke for a given geometry and rotational speed. Then the losses, efficiency, torque density, and power density are calculated on MATLAB using the FEA model output values. Table I lists the parameters and performance metrics of the 10MW and 200kW generator designs.

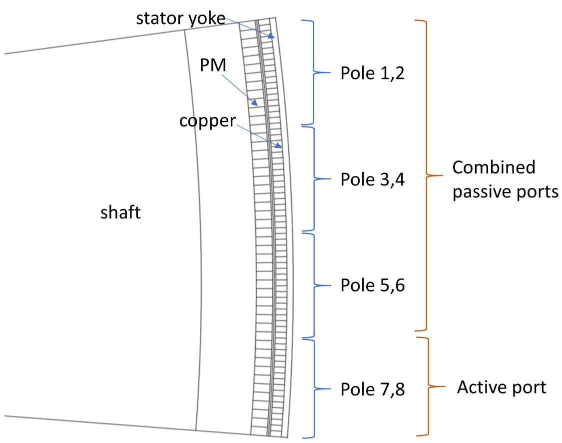

Fig. 2: Schematic showing the generator port layout

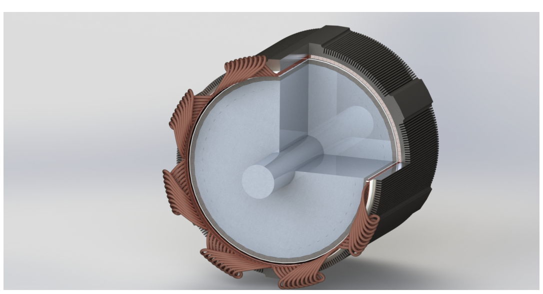

Fig. 3: Prototype CAD model cross sectional view

A. Winding Design

The slotless PM machines is designed for the main flux to pass through the stator windings. Thus, it is necessary to strand the stator copper, such that eddy current losses due to the varying airgap flux are minimized. Litz wire constructed of thin copper strands with transposed bundling are thus utilized for the generator windings. The requirements on strand size and bundle design depends on the conductor size and the maximum operating frequency of the machine.

TABLE I: Design Parameters of the 10 MW and 200 kW Multi-Port Generator

Parameters	10 MW Design	200kW Design
Speed (RPM)	9.6	3600
Pole Count	240	16
Electrical Frequency (Hz)	19.2	480
Shaft Radius (mm)	6000	150
Magnet Thickness (mm)	68.4	8.6
Airgap Thickness (mm)	10	3.5
Winding Thickness (mm)	35.8	6.1
Stator Yoke Thickness (mm)	25.7	6.5
Current Density (A_{rms}/mm^2)	3.2	7.8
Axial Stack Length (mm)	1365	284
Outer Diameter (cm)	1259	38
Magnet Weight (kg)	27219	19
Active Weight (kg)	64100	61
Copper Loss (W)	280138	2398
Iron Loss (W)	12222	519
Total Loss (W)	292360	3243
Efficiency (%)	97.2	98.4
Power Density (W/kg)	158	3301
Torque Density (Nm/Kg)	157	9

From an AC loss perspective, the machine benefits from a Litz wire with the smallest strand size. Although a thin strand size would nearly eliminate the AC losses, using it results in a relatively flexible conductor. As a result, winding Litz wire into a form-wound motor coil requires additional effort with mold design and impregnating it with a resin that provides additional mechanical strength. Form-wound Litz coils with a flexible Litz wire are discussed in [7]–[9].

Considering the fundamental frequency of 480 Hz, a rigid Litz wire composed of a large strand size is explored to simplify manufacturing efforts. A custom-made type 8 square-shaped Litz wire with heavy built 17 AWG magnet wire was thus selected [10]. The DC and AC copper losses can be computed as [11]:

$$P_{dc} = I_{rms}^2 R_{dc} \tag{1}$$

$$P_{ac} = \frac{\pi \omega_0^2 B^2 n d_s^4 l_{act}}{128 \rho_{cu}} \left(1 + \frac{n \pi^2 d_s^2}{4 k_{cu} p_{opt}^2}\right) \tag{2}$$

where B represents the spatial average of peak flux density, ω_0 is the angular frequency, n is the strand number, d_s is the strand diameter, l_{act} is the active length, ρ_{cu} is the copper resistivity, k_{cu} is the copper fill factor, and p_{opt} is the optimum strand pitch. Figure 4 shows the copper loss variation as a function of strand number for the generator. From the figure, using 25 strands per coil would keep the AC copper losses below 5-10% of the DC copper loss.

The winding pattern is designed to meet the unique phase-shifted back-emf requirement of 20° between each phase. The winding diagram shown in Fig. 5 is used in the machine to achieve the multi-port architecture with the required phase distribution. The difference in coil pitch in the active port windings versus the passive port windings demand different

979-8-3315-8138-1

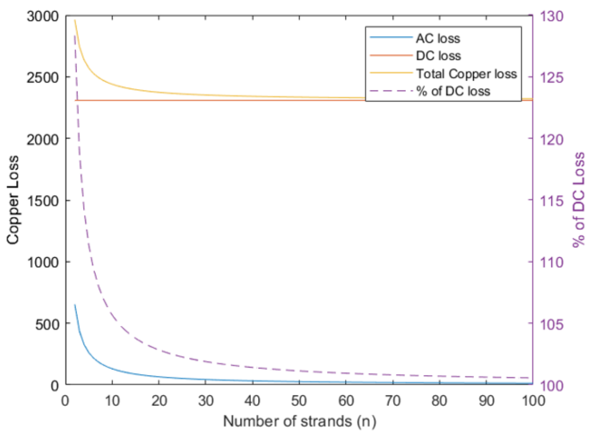

Fig. 4: AC copper loss analysis

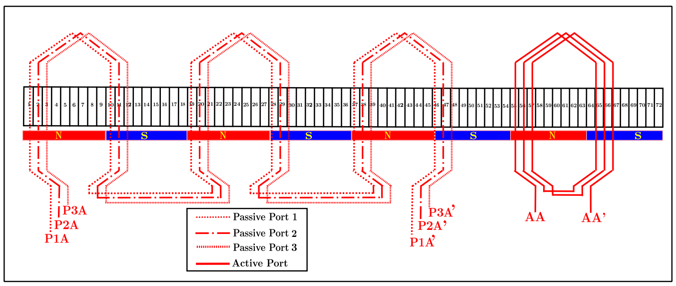

Fig. 5: Winding diagram showing the Phase A winding layout for the different ports of the generator

bending radii in the end-winding sections. In order to meet the required bend radius of the Litz bundle without debraiding it, a specially designed wire bending rig was used.

B. Thermal Design

The 200 kW generator prototype was designed to operate using air cooling. Additional fins were designed on the stator yoke outer surface to increase the surface area for heat dissipation, based on calculations from the 1-D thermal circuit shown in the Fig. 6. The 1-D thermal model assumes the heat generated in the copper winding is dissipated only through the outer surface. Heat dissipation through the airgap and the end windings was neglected. With this assumption, the hot spot temperature is at the inner radius of the copper windings in the stator. The 1-D thermal circuit has resistances arising from the copper winding, enamel insulation, slot liner, stator yoke, and

TABLE II: Insulation materials used in the windings

Insulation	Material	Thickness (mm)	Thermal Conductivity (W/mK)
copper enamel	Heavy Polyester Polyamideimide	0.09	0.259
slot liner	NOMEX®410	0.25	0.157

yoke-air interface. Copper and enamel insulation thicknesses were calculated based on the magnet wire datasheet [10]. Since the generator radial dimensions were fixed, the only variable available to reduce the hot spot temperature to 120 $°C$ (calculated based on the rated temperature of the permanent magnets) was the surface area of the yoke. Therefore, the number of fins (and hence the surface area) was decided based on the required convection thermal resistance calculated in equation 3.

$$R_{conv} = \frac{1}{h_{stator} A_{finarea}} \tag{3}$$

III. Construction of 200-kW PMSG

A. Rotor Construction

Manufacturability concerns were addressed in the PM and winding sizing for the final design. To assure the magnets were evenly distributed along the circumference of the rotor surface, a 10 mil notch was introduced. The change in slot height has a direct implication on the losses and efficiency of the machine, as well as torque density. FEM was modified to introduce these detailed design changes that arose due to manufacturing limits which are reflected in the specifications in Table I.

The permanent magnet rotor uses a Halbach array pattern of 6 magnet segments per pole, each with the magnetization direction angled 30 degrees apart. The resulting near-sinusoidal back-emf is essential for the operation of the multi-port rectifier architecture. However, manufacturing the rotor by gluing six magnet pieces with different magnetization directions increases the overall complexity of rotor manufacturing.

B. Stator Construction

The electrical frequency of the generator is 480 Hz. This frequency is 25 times higher than the electrical frequency of the 10 MW generator design. Given this, the 200 kW prototype will have significant AC conductor losses, making the use of stranded copper conductors imperative. Nomex paper was used as phase-to-phase and phase-to-ground insulation. The completed winding was impregnated using an epoxy resin. Phase-to-phase and phase-to-ground Nomex insulation were carefully extended to cover the bending region between the end windings and the active winding length. In this case, it was also the Nomex insulation. This is required in slotless machines since, compared to slotted machines, slotless machines lack significant space between the phase windings exiting the active part of the machine.

IV. Experimental Results

A. Electromagnetic design

The Figure 8 shows the constructed generator. It has 48 terminals in total. The mutual inductance in this generator significantly influences the rectifier output current ripple. Therefore, the mutual inductance was measured in each phase.

979-8-3315-8138-1

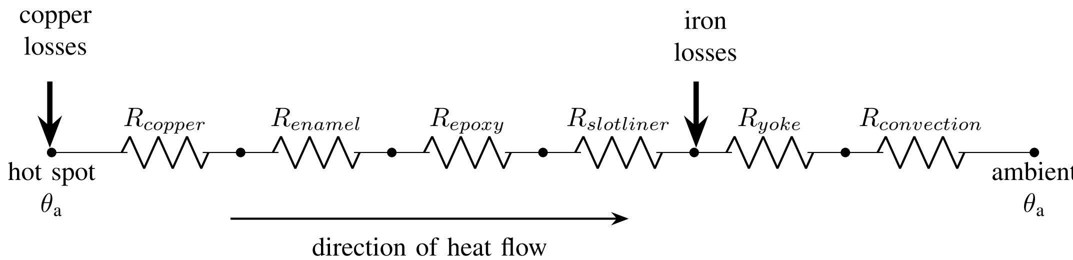

Fig. 6: 1-D thermal equivalent circuit

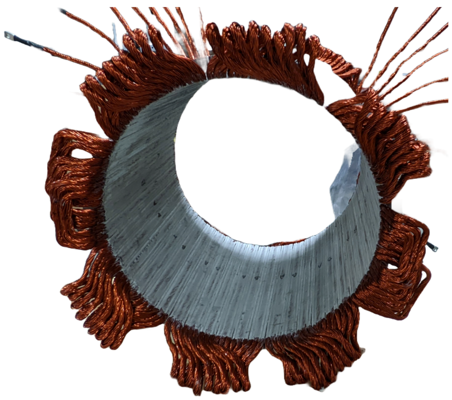
Fig. 7: Stator with litz wire

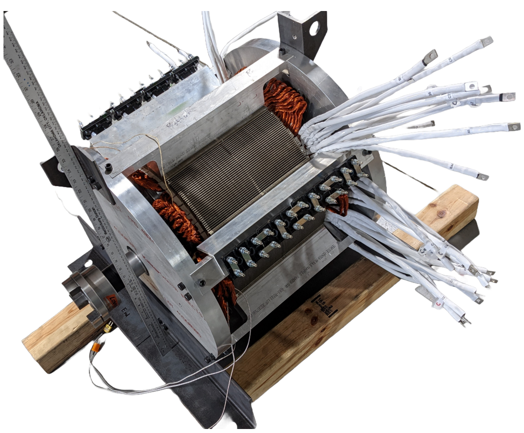
Fig. 8: Final generator prototype

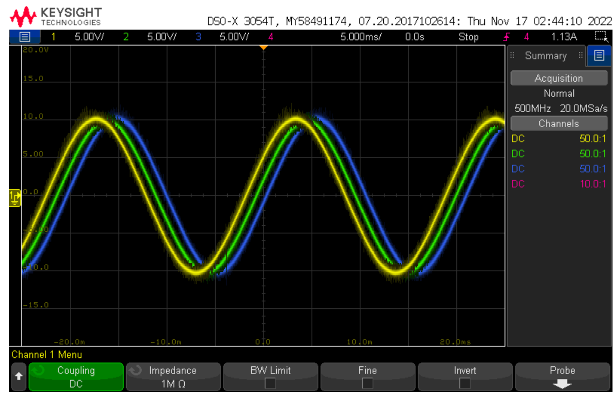

Fig. 9: Experimental back emf of phase A of each of the three passive ports

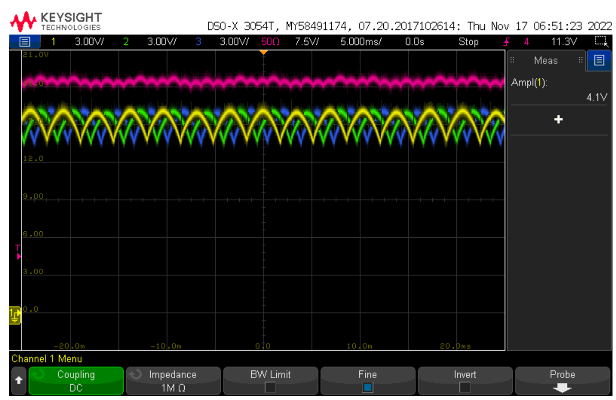

Fig. 10: DC output current waveform

Once the construction was completed, the stator windings' thicknesses and air gap were measured to verify accuracy. A spin test at 3600 rpm was done to ensure the rotor stability and that the retaining ring is strong enough to retain the magnets. The back emf test was conducted to measure the back emf constant and phase shift of each phase. The results are shown in the Fig. 9 and 10.

B. Thermal performance

The thermal performance of the generator was tested to ensure the winding hot spot temperature stays within the design limit. The motor has thermocouples connected to the end winding of each phase in every port to measure the end winding temperature during testing. However, during testing, the setup is enclosed in a safety chamber, which limits air circulation. Therefore, additional fans were mounted on the generator to cool the generator during testing. To study the thermal performance of the generator under natural convection conditions, the generator stator temperature was measured by applying a DC current through each winding, and the cooling fans were kept off. Table III shows the measured end winding temperature at 100 A and 200 A. Then, the temperatures were measured at 100 A, 200 A, and 300 A under forced convection conditions with the cooling fans turned on. The comparison of the 1-D thermal model and the actual

979-8-3315-8138-1

measurements are also shown in Table III. The 1-D thermal model calculated the temperature inside the motor, whereas the measured values correspond to the end winding. Therefore, to validate the measurements, a thermal model of the motor was simulated on COMSOL. The measured and simulated temperature distribution inside the wingings at 200A is shown in Fig. 11 and Fig. 12 respectively. The hot spot temperature was observed at the end windings.

TABLE III: Measured and Calculated Winding Temperatures

Cooling	Current (A)	Measured Temperature (°C)	Calculated Temperature (°C)
Natural Convection	100	38.2	44.8
	200	71.5	108.0
Forced Convection	100	30.2	32.0
	200	41.2	53.3
	300	62.0	97.3

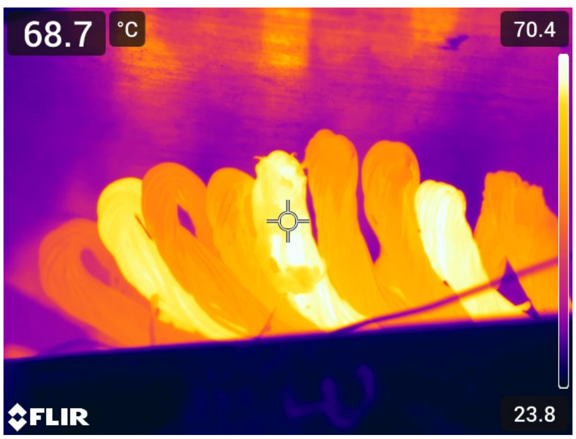

Fig. 11: Measured temperature distribution in the end winding

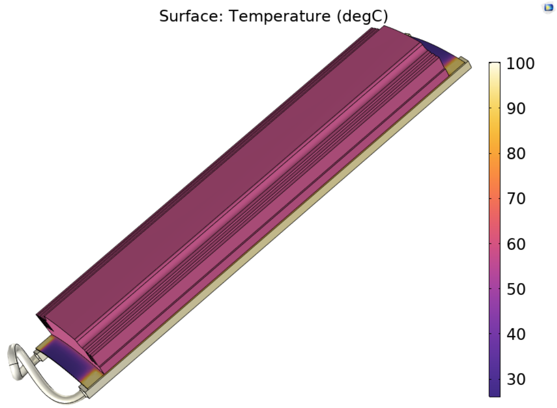

Fig. 12: FEA simulated temperature distribution in the end winding at 200 A without cooling

V. Conclusion

This paper presented the optimization, design, and construction of a 200 kW multi-port slotless PMSG prototype achieving a design efficiency of 97.2% and a torque density of 9 Nm/kg. The machine was developed to demonstrate the feasibility of an MW-class multi-port integrated generator–rectifier architecture at the kW scale. Key manufacturing challenges and the resulting design modifications were outlined, and the prototype's thermal and electromagnetic behavior was evaluated and shown to align well with FEA predictions. The results validate the feasibility of the integrated generator–rectifier concept at this power level. Future work will involve full-power testing of the 200 kW PMSG in conjunction with the integrated rectifier system to experimentally verify overall system performance.

VI. Acknowledgement

This work was supported by the Advanced Research Projects Agency–Energy (ARPA-E), U.S. Department of Energy, under Award No. DE-AR0001057. The authors would like to thank Jerry Shannon and Patrick McCleer of McCleer Power LLC, Jackson MI, for their support in the construction of the prototype.

References

[1] S. W. D. Thusara Samith Sirimanna, "Design of 10 mw low inductance pm generator for direct drive offshore wind turbine," Master's thesis, University of Illinois Urbana-Champaign, 2020.

[2] P. Huynh, S. Sirimanna, J. Mok, D. Lee, O. Ajala, S. Linares, D. Mulas, K. Haran, A. Dominguez-Garcia, G. Gross, and A. Banerjee, "Integrated generator-rectifier co-design for offshore wind turbines," in *2020 IEEE Energy Conversion Congress and Exposition (ECCE)*, 2020, pp. 4194–4201.

[3] P. Huynh and A. Banerjee, "Active voltage-ripple compensation in an integrated generator-rectifier system," *IEEE Transactions on Power Electronics*, vol. 36, no. 2, pp. 2270–2282, 2021.

[4] P. Huynh, S. Tungare, and A. Banerjee, "Maximum power point tracking for wind turbine using integrated generator–rectifier systems," *IEEE Transactions on Power Electronics*, vol. 36, no. 1, pp. 504–512, 2021.

[5] D. Lee, S. Sirimanna, P. T. Huynh, E. Libbos, A. Banerjee, and K. S. Haran, "Slotless-pm machine design for an integrated generator-rectifier architecture for off-shore wind turbines," *IEEE Journal of Emerging and Selected Topics in Power Electronics*, vol. 10, no. 2, pp. 1745–1755, 2022.

[6] S. Sirimanna, P. Huynh, A. Samarakoon, D. Lee, A. Banerjee, and K. Haran, "Design and optimization of an integrated generator-rectifier system for offshore wind turbines," in *2021 IEEE International Electric Machines & Drives Conference (IEMDC)*, 2021, pp. 1–6.

[7] T. Balachandran, S. Srimmana, A. Anderson, X. Yi, N. Renner, and K. S. Haran, "Assembly and qualification of a slotless stator assembly for a mw-class permanent magnet synchronous machine," in *2020 AIAA/IEEE Electric Aircraft Technologies Symposium (EATS)*, 2020, pp. 1–10.

[8] D. Lee, T. Balachandran, S. Sirimanna, N. Salk, A. Yoon, P. Xiao, J. Macks, Y. Yu, S. Lin, J. Schuh, P. Powell, and K. S. Haran, "Detailed design and prototyping of a high power density slotless pmsm," *IEEE Transactions on Industry Applications*, vol. 59, no. 2, pp. 1719–1727, 2023.

[9] T. Balachandran, S. Sirimmana, A. Jin, and K. S. Haran, "Partial discharge testing of form-wound air-core armature windings for a high-frequency pmsm for electric aircraft applications," in *2018 IEEE International Conference on Information and Automation for Sustainability (ICIAfS)*, 2018, pp. 1–6.

[10] *Magnet wire / winding wire engineering data handbook*, Essex Furukawa Magnet Wire LLC, 12 2009, rev. 1.

[11] J. Martin, A. Yoon, A. Jin, and K. S. Haran, "High-frequency litz "air-gap" windings for high-power density electrical machines," *Electric Power Components and Systems*, vol. 45, no. 7, pp. 798–805, 2017.